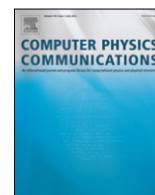




Contents lists available at ScienceDirect

Computer Physics Communications

journal homepage: www.elsevier.com/locate/cpc

MATLAB-based program for optimization of quantum cascade laser active region parameters and calculation of output characteristics in magnetic field[☆]



J. Smiljanić^{a,b,*}, M. Žeželj^{a,b}, V. Milanović^b, J. Radovanović^b, I. Stanković^a

^a Scientific Computing Laboratory, Institute of Physics Belgrade, University of Belgrade, Pregrevica 118, 11080 Belgrade, Serbia

^b School of Electrical Engineering, University of Belgrade, Bulevar Kralja Aleksandra 73, 11120 Belgrade, Serbia

ARTICLE INFO

Article history:

Received 21 March 2013

Received in revised form

21 October 2013

Accepted 23 October 2013

Available online 31 October 2013

Keywords:

Quantum cascade laser

Scattering

LO-phonons

Interface roughness

MATLAB program

ABSTRACT

A strong magnetic field applied along the growth direction of a quantum cascade laser (QCL) active region gives rise to a spectrum of discrete energy states, the Landau levels. By combining quantum engineering of a QCL with a static magnetic field, we can selectively inhibit/enhance non-radiative electron relaxation process between the relevant Landau levels of a triple quantum well and realize a tunable surface emitting device. An efficient numerical algorithm implementation is presented of optimization of GaAs/AlGaAs QCL region parameters and calculation of output properties in the magnetic field. Both theoretical analysis and MATLAB implementation are given for LO-phonon and interface roughness scattering mechanisms on the operation of QCL. At elevated temperatures, electrons in the relevant laser states absorb/emit more LO-phonons which results in reduction of the optical gain. The decrease in the optical gain is moderated by the occurrence of interface roughness scattering, which remains unchanged with increasing temperature. Using the calculated scattering rates as input data, rate equations can be solved and population inversion and the optical gain obtained. Incorporation of the interface roughness scattering mechanism into the model did not create new resonant peaks of the optical gain. However, it resulted in shifting the existing peaks positions and overall reduction of the optical gain.

Program summary

Program title: QCL

Catalogue identifier: AERL_v1_0

Program summary URL: http://cpc.cs.qub.ac.uk/summaries/AERL_v1_0.html

Program obtainable from: CPC Program Library, Queen's University, Belfast, N. Ireland

Licensing provisions: Standard CPC licence, <http://cpc.cs.qub.ac.uk/licence/licence.html>

No. of lines in distributed program, including test data, etc.: 37763

No. of bytes in distributed program, including test data, etc.: 2757956

Distribution format: tar.gz

Programming language: MATLAB.

Computer: Any capable of running MATLAB version R2010a or higher.

Operating system: Any platform supporting MATLAB version R2010a or higher.

RAM: Minimum required is 1 GB. Memory usage increases for less intense magnetic fields.

Classification: 15.

[☆] This paper and its associated computer program are available via the Computer Physics Communication homepage on ScienceDirect (<http://www.sciencedirect.com/science/journal/00104655>).

* Corresponding author at: Scientific Computing Laboratory, Institute of Physics Belgrade, University of Belgrade, Pregrevica 118, 11080 Belgrade, Serbia. Tel.: +381 113713152.

E-mail address: jelena.smiljanic@ipb.ac.rs (J. Smiljanić).

Nature of problem:

The nature of the problem is to provide an efficient numerical algorithm implementation for optimization of GaAs/AlGaAs QCL active region parameters and calculation of output properties in the magnetic field.

Solution method:

The optimization of the QCL laser performance at selected wavelength is performed at entire free-parameters space using simulated annealing algorithm. The scattering rates are calculated in the presence and without magnetic field and used as coefficients in rate equations. The standard MATLAB procedures were used to solve iteratively this system of equations and obtain distribution of electron densities over electronic states.

Restrictions:

The machine must provide the necessary main memory which decreases roughly quadratically with the increase of the magnetic field intensity.

Running time:

Optimization time on Intel 3 GHz processor is about 2×10^4 s. The calculation time of laser output properties for values set automatically in GUI is 5×10^4 s.

© 2013 Elsevier B.V. All rights reserved.

1. Introduction

Molecular beam epitaxy (MBE) technique [1], allowed the realization of complex heterostructures, with the quantum well as a basic structural building block. The inherent design variability of these structures gave rise to a new direction of research that relies on the so-called band-structure engineering. In superlattices comprising many coupled quantum wells, energy subbands are formed in analogy with what happens when atoms are brought together to form a solid [2]. The first intersubband heterostructure laser was created by Jerome Faist et al. [3]. In recent years the scientific community has witnessed a rapid progress in the development of semiconductor quantum cascade lasers (QCLs) [4–8]. The optimization of the structure and prediction of performance of the QCL is an important contribution of theory to the development [9–14].

Quantum cascade lasers have become light sources of choice for a broad variety of applications including high-sensitivity gas sensing, infrared imaging, military countermeasures, security monitoring, non-invasive medical diagnostics, optical communications [3,4,15–19]. In the mid- and far-infrared spectral range, these powerful light sources are particularly appreciated for the wide scope of operating wavelengths which can be achieved by using the same heterostructure material combination. Some of the features that make this kind of device so unique are: unipolarity, the population inversion achieved through careful quantum engineering of the lifetimes of the states (typically in the ps range) and the electron recycling due to the cascading scheme. Their performance under the influence of high magnetic field has been intensively studied as well, due to the fact that magnetic field may serve as an efficient tool to determine the nature and magnitude of the scattering mechanisms in the active region [5–8,20–24]. Early experiments have demonstrated QCL emission enhancement and a magneto-phonon-resonance effects [5–7] which have led to a deeper insight into the physics of intersubband lasers. Furthermore, in the THz frequency range where the performances of QCLs deteriorate rapidly with temperature, due to detrimental thermal activation of non-radiative losses, the highest operating temperature of 225 K is reported for the structure assisted by external magnetic field for additional carrier confinement [21]. Recently, a portable QCL based infrared magnetospectrometer covering the spectral range from 5 to 120 μm has been presented, for applications in cyclotron-resonance spectroscopy measurements where high magnetic fields (up to 60 T) are required [16]. Hence, a detailed understanding of various scattering mechanisms under the influence of strong magnetic field is an important factor for improving QCL performances and applicability.

The typical design of the QCL active region entails a three-level system. The carriers are injected into the upper laser state, from which they can relax into the lower state by means of photon-assisted transition or by scattering, mainly by interactions with LO-phonons. In order to achieve the population inversion the lifetimes of electrons in the quantum states must satisfy the relation $\tau_{32} > \tau_{21}$: this condition is achieved by means of two key points. The lifetime τ_{21} is reduced by making the energy E_{21} resonant with the optical phonon energy, which is the most efficient scattering mechanism. The lifetime τ_{32} is increased by employing a transition with a reduced spatial overlap of the wavefunctions. Further extension of otherwise short carrier lifetime (of the order of 1 ps) is achieved using an intense magnetic field parallel to the growth direction of semiconductor layers [6–8,20]. The magnetic field breaks the two-dimensional (2D) in-plane continuous energy subbands into discrete Landau levels. The lifetime of electrons in the excited laser state is strongly modulated by the applied magnetic field. The dependence of electron lifetime on magnetic field intensity results in oscillations in the laser emission intensity. The inelastic scattering by LO-phonons and elastic scattering by interface roughness were identified as main mechanisms behind this effect by Leuliet et al. [8]. Given that the scattering processes between the two states depend on their energy spacing, certain relaxation mechanisms can be enhanced or inhibited by varying the magnetic field strength, although they may be influenced by the operating temperature as well. LO-phonon scattering is well explained in previous theoretical and experimental works [6–8,20,25]. Increasing magnetic field reduces the number of relevant Landau levels and changes the energy differences between individual levels, thus affecting the lifetime of carriers in higher states. On the other hand, the influence of interface roughness scattering has only recently been studied in detail [26]. The strength of the interface roughness scattering in a particular sample is determined by the morphology of the interfaces. In contrast to LO-phonon, interface roughness (IR) scattering does not depend on the temperature. As a result, efficiency of interface roughness scattering mechanism remains constant with increasing temperature, while the efficiency of LO-phonon scattering is reduced due to their higher absorption [27].

The purpose of the present paper is to give a simple and efficient program for the numerical solution of the rate equations based model and analysis of the optical gain in the active region of the QCL in magnetic field. An easy-to-use MATLAB[®] user interface is provided. In order to find an optimal design of the structure for operation at specific wavelength and temperature, optimization procedure is provided as well. The procedures for calculation of

LO-phonon and IR scattering rates are also included both with and without magnetic field. The electron distribution over the states of the system is found by solving the full set of rate equations which describe the transitions between levels, and subsequently used to determine the optical gain. These results can be easily calculated by a moderate PC configuration using the MATLAB[®] programs provided, due to efficient numerical implementation. This is important, since the number of levels involved is inversely proportional to the applied magnetic field.

In Section 2, we present a theoretical description of QCL active region and introduce models for LO-phonon and IR scattering rate with and without the presence of an external magnetic field. The rate equations which describe the population change of each Landau level are presented as well. The stationary solution of these equations allows for evaluating the population inversion and the resulting optical gain. In Section 3 we present a description of the MATLAB[®] program, an explanation about inputs and how to use the graphical user interface. In Section 4, we demonstrate the program features by calculating the optimal QCL active region parameters at different wavelengths. The calculations are also presented for the scattering rates and the total relaxation rate from the upper laser state, for a wide range of magnetic fields (3–60 T) and two temperatures $T = 77$ and 300 K. By using the calculated scattering rates as input data, rate equations are solved and population inversion and the optical gain are obtained. For both the population inversion and the gain, interface roughness scattering is shown to have a significant influence in terms of reducing the predicted magnitude, especially at low temperatures. Finally, in Section 5 we present a brief summary of our work.

2. Theoretical considerations

The active region of the QCL structure under consideration comprises three coupled quantum wells (QWs) biased by an external electric field \vec{E} . In the absence of the magnetic field this system has three energy states, i.e., subbands ($n = 1, 2, 3$), and the laser transition occurs between subbands $n = 3$ and $n = 2$. This active region is surrounded by suitable emitter/collector regions in the form of superlattices, designed as Bragg reflectors, which inject electrons into state $n = 3$ on one side, and allow for rapid extraction of carriers from the lowest subband $n = 1$, on the other side. The energy difference between E_2 and E_1 should match the LO-phonon energy in order to ensure fast depopulation via LO-phonon scattering and maintain a short lifetime for the lower laser level. In addition, we introduce in our calculations the interface roughness scattering as an additional non-radiative relaxation mechanism.

In the absence of an external magnetic field, the electronic subbands have a free particle-like energy dispersion in the direction parallel to the QW planes $E_n + \hbar^2 k_{\parallel}^2 / 2m_{\parallel n}(E_n)$, where $m_{\parallel n}(E_n)$ is the energy-dependent in-plane wave vector. However, when this structure is subjected to a strong magnetic field B in the z -direction, continuous subbands transform into series of individual (strictly discrete) states, the total energies of which are [7] $E_{n,l} \approx E_n + (l + 1/2)\hbar\omega_{c_n}$ where $l = 0, 1, 2, \dots$ is the Landau index, $E_n \equiv E_n(k_{\parallel} = 0)$, the term $(l + 1/2)\hbar\omega_{c_n}$ originates from the in-plane kinetic energy part of the subband, and $\omega_{c_n} = eB/m_{\parallel n}$ is the corresponding cyclotron frequency. The values of B which give rise to resonant LO-phonon emission are found by solving the equation $E_{3,0} - E_{n,l} = \hbar\omega_{LO}$ where $n = 1, 2$, while $\hbar\omega_{LO}$ is the LO-phonon energy.

According to [8,20], to account for the variations of the well widths, a Gaussian probability density is introduced:

$$\Pi(L_i) = \frac{1}{\sigma\sqrt{2\pi}} e^{-(L_i - L_{i0})^2 / 2\sigma^2} \quad (1)$$

for the i th well width L_i , $i = 1, 2, 3$. In order to keep the results as analytical as possible, we assume that around a mean value L_{i0} the

energy difference varies linearly with L_i , i.e.

$$E_{n_i, l_i}(L_i) - E_{n_f, l_f}(L_i) \approx E_{n_i, l_i}(L_{i0}) - E_{n_f, l_f}(L_{i0}) - \gamma(L_i - L_{i0}) \quad (2)$$

with the factor γ taken the same for all Landau levels, according to [8,20].

By introducing Eqs. (1) and (2) into the Fermi golden rule, we obtain the following function:

$$\begin{aligned} J^s &= \int_{-\infty}^{\infty} \Pi(L_i) \delta[E_{n_i, l_i} - E_{n_f, l_f} - \Delta E_s] dL_i \\ &= \frac{1}{\delta\sqrt{2\pi}} e^{-(E_{n_i, l_i} - E_{n_f, l_f} - \Delta E_s)^2 / 2\delta^2}, \end{aligned} \quad (3)$$

where $\delta = \sigma\gamma$ is the width of the Gaussian distribution of energy difference $E_{n_i} - E_{n_f} + (l_i\omega_{c_{n_i}} - l_f\omega_{c_{n_f}})\hbar + \hbar(\omega_{c_{n_i}} - \omega_{c_{n_f}})/2 - \Delta E_s$, and s denotes the scattering mechanism (electron–LO-phonon scattering (LO) or interface roughness (IR) scattering). In our notation $\Delta E_{LO} = \hbar\omega_{LO}$ and $\Delta E_{IR} = 0$. The terms $E_{n,l}$ represent the total energies of Landau levels and a more detailed explanation of their calculation will be provided in the continuation of this section (see Eq. (19)).

The material parameters for GaAs used in the calculation are $m_{\text{GaAs}} = 0.067m_0$ and for AlAs $m_{\text{AlAs}} = 0.15m_0$ (m_0 is the free electron mass), effective mass in $\text{Al}_x\text{Ga}_{1-x}\text{As}$ is $m = xm_{\text{AlAs}} + (1-x)m_{\text{GaAs}}$. The dielectric permittivities used in the numerical calculations are $\epsilon_{\infty} = 10.67$, $\epsilon_s = 12.51$ and $\delta = 6$ meV.

2.1. Electron–LO-phonon scattering in magnetic field

The electron–LO-phonon scattering rates for phonon emission between the initial state E_{n_i, l_i} and the final state E_{n_f, l_f} may be found from

$$\begin{aligned} \frac{1}{\tau_{(n_i, l_i) \rightarrow (n_f, l_f)}^{LO}} &= \frac{1}{\hbar} \sum_{\vec{q}} |\langle n_f, l_f, k_{x_f}, n_q + 1 | \hat{H}_{e-ph}(\vec{q}) | n_i, l_i, k_{x_i}, n_q \rangle|^2 J^{LO}. \end{aligned} \quad (4)$$

In this expression, electron–LO-phonon Hamiltonian $\hat{H}_{e-ph}(\vec{q})$ is the sum of the interaction Hamiltonians with each phonon mode defined by its 3D wave vector \vec{q} , see [20], and k_{x_i} and k_{x_f} are the initial and the final state wave vector components, respectively. From the previous equation one obtains the following analytical expression for the scattering rate:

$$\begin{aligned} \frac{1}{\tau_{(n_i, l_i) \rightarrow (n_f, l_f)}^{LO, e}} &= \frac{e^2\omega_{LO}}{4\epsilon_0} \left(\frac{1}{\epsilon_{\infty}} - \frac{1}{\epsilon_s} \right) \\ &\times \frac{1}{\delta\sqrt{2\pi}} e^{-(E_{n_i, l_i} - E_{n_f, l_f} - \hbar\omega_{LO})^2 / 2\delta^2} (n_q + 1) \\ &\times \int_0^{\infty} |F(q_{\parallel})|^2 G(q_{\parallel}) dq_{\parallel}, \end{aligned} \quad (5)$$

where ϵ_{∞} and ϵ_s are the static and the high-frequency relative dielectric constant, respectively, ϵ_0 is the vacuum dielectric permittivity and $n_q = [\exp(\hbar\omega_{LO}/k_B T) - 1]^{-1}$ is the mean number of LO-phonons. Furthermore, q_{\parallel} is the in-plane component of the phonon wave vector $\vec{q} = (q_z, q_{\parallel})$ and $F(q_{\parallel})$ is the lateral overlap integral

$$|F(q_{\parallel}, l_i, l_f)|^2 = e^{-(q_{\parallel}^2/2\beta^2)} \frac{l_i!}{l_f!} \left(\frac{q_{\parallel}^2}{2\beta} \right)^{l_f - l_i} \left[L_{l_i}^{l_f - l_i} \left(\frac{q_{\parallel}^2}{2\beta} \right) \right]^2, \quad (6)$$

where $\beta = \sqrt{eB/\hbar}$ is the magnetic length and $L_m^k(x)$ represents the associate Laguerre polynomial [28]. Finally, $G(q_{\parallel})$ stands for the

form factor given by

$$G(q_{\parallel}) = \int \int \eta_i^*(z) \eta_f(z) \eta_i(z') \eta_f^*(z') e^{-q_{\parallel}|z-z'|} dz dz', \quad (7)$$

where η_i and η_f denote the z -dependent parts of the electronic wave functions. The electron-LO-phonon scattering rate for phonon absorption [29] is

$$\frac{1}{\tau_{(n_f, l_f) \rightarrow (n_i, l_i)}^{LO, [a]}} = \frac{1}{\tau_{(n_i, l_i) \rightarrow (n_f, l_f)}^{LO, [e]}} \frac{1}{e^{\hbar\omega_{LO}/kT}}. \quad (8)$$

Phonon absorption is significant at room temperature ($T = 300$ K) and it almost vanishes at low temperatures ($T = 77$ K).

2.2. Electron-LO-phonon scattering without the magnetic field

When the magnetic field is not present, the electron-LO-phonon scattering rate may be evaluated from

$$\frac{1}{\tau_{if}^{LO}(B=0)} = \frac{2\pi}{\hbar} \sum_{\vec{q}} \left| \langle n_f, \vec{k}_f, n_q \right. \\ \left. + 1 | \hat{H}_{e-ph}(\vec{q}) | n_i, \vec{k}_i, n_q \rangle \right|^2 J^{LO}. \quad (9)$$

The Hamiltonian \hat{H}_{e-ph} is in this case the sum of interaction Hamiltonians with each phonon mode defined by its 3D wave vector \vec{q} , see [30], and \vec{k}_i and \vec{k}_f are the initial and the final state in-plane wave vectors, respectively. From the previous equation one obtains the following expression for the scattering rate in the absence of magnetic field:

$$\frac{1}{\tau_{if}^{LO}(B=0)} = \frac{e^2 \omega_{LO} m}{4\pi \hbar^2 \epsilon_0} \left(\frac{1}{\epsilon_{\infty}} - \frac{1}{\epsilon_s} \right) (n_q + 1) \int_0^{\pi} \frac{G(q_{\parallel})}{q_{\parallel}} d\theta, \quad (10)$$

where $G(q_{\parallel})$ and q_{\parallel} are the form factor and the in-plane component of phonon wave vector, respectively. The form factor is already defined in Eq. (7) and $q_{\parallel}^2 = 2m(E_i - E_f - \hbar\omega_{LO})/\hbar^2$.

2.3. IR scattering in magnetic field

We use the model for interface roughness scattering proposed by Leuliet et al., cf. [8]. This model assumes the in-plane terrace-like surface defects, as explained in [31]. In order to evaluate the interface roughness scattering rate, we introduce spatial distribution of roughness which follows the Gaussian correlation function [8,32–34,29]:

$$\langle \Delta(\vec{r}) \Delta(\vec{r}') \rangle = \Delta^2 e^{-|\vec{r}-\vec{r}'|^2/\Lambda^2}, \quad (11)$$

with Δ being the mean height of the roughness and Λ the correlation length. We also introduce the corresponding perturbation Hamiltonian [8],

$$\hat{H}_{IR} = U_0 \delta(z - z_i) \Delta(x, y), \quad (12)$$

where U_0 is the barrier height at interface position z_i .

The electron-interface roughness scattering rate can be calculated from the following expression:

$$\left\langle \frac{1}{\tau_{(n_i, l_i) \rightarrow (n_f, l_f)}^{IR}}(z_i) \right\rangle \\ = \frac{2\pi}{\hbar} \left\langle \sum_{k_{x_i}, k_{x_f}} \left| \langle n_f, l_f, k_{x_f} | \hat{H}_{IR} | n_i, l_i, k_{x_i} \rangle \right|^2 \right\rangle J^{IR}. \quad (13)$$

In the above expression, the averaging is performed over space (as follows from Eq. (11)), and over the initial state wave vector

component k_{x_i} :

$$\frac{1}{\tau_{n_i, l_i \rightarrow n_f, l_f}^{IR}} = \frac{\sqrt{2}}{\hbar \delta} e^{-\frac{(E_{n_i, l_i} - E_{n_f, l_f})^2}{2\delta^2}} \times |F_{if}|^2 \Delta^2 \Lambda \alpha \\ \times \int_{-\infty}^{+\infty} e^{-\frac{\Delta k_x^2}{2}} \left[\frac{2 + \Lambda^2 \beta^2}{2\beta^2} \right] \zeta(\Delta k_x) d(\Delta k_x). \quad (14)$$

Here, $\Delta k_x = k_{x_i} - k_{x_f}$, $F_{if} = U_0 \eta_i^*(z_i) \eta_f(z_i)$ and $\alpha = \beta^2 / (\pi l_f! l_i! 2^{l_f+l_i})$. The form factor $\zeta(\Delta k_x)$ is given by:

$$\zeta(\Delta k_x) = \int \int \exp \left(-\beta^2 [t^2 + (t - \omega)^2] - \frac{\omega^2}{\Lambda^2} \right) \\ \times H_{l_i} \left[\beta t - \frac{\Delta k_x}{2\beta} \right] H_{l_i} \left[\beta(t - \omega) - \frac{\Delta k_x}{2\beta} \right] \\ \times H_{l_f} \left[\beta t + \frac{\Delta k_x}{2\beta} \right] H_{l_f} \left[\beta(t - \omega) + \frac{\Delta k_x}{2\beta} \right] dt d\omega \quad (15)$$

and H_j is the Hermite polynomial of order j .

2.4. IR scattering without magnetic field

The electron-interface roughness scattering rate can be calculated from the following expression:

$$\left\langle \frac{1}{\tau_{n_i \rightarrow n_f}^{IR}}(z_i) \right\rangle = \frac{2\pi}{\hbar} \left\langle \sum_{k_i, k_f} \left| \langle n_f, \vec{k}_f | \hat{H}_{IR} | n_i, \vec{k}_i \rangle \right|^2 \right\rangle J^{IR}. \quad (16)$$

The Hamiltonian \hat{H}_{IR} is the same as in the case with magnetic field, i.e., Eq. (12). The averaging is performed over space, and over amplitude of the initial k_i and the final k_f state wavevector. The following expression for IR scattering rate without magnetic field is obtained:

$$\left\langle \frac{1}{\tau_{if}^{IR}(B=0)} \right\rangle = \frac{\sqrt{2\pi}}{\hbar \delta} e^{-\frac{(\Delta E_{if})^2}{2\delta^2}} \frac{1}{4} |F_{if}|^2 (\Delta \Lambda)^2 \\ \times \int_0^{+\infty} e^{-\frac{\hbar^4}{4m^2} x^2 - \left[\frac{\Lambda^2}{4} - \frac{\hbar^2}{m} \frac{\Delta E_{if}}{2\delta^2} \right] x} dx. \quad (17)$$

2.5. Rate equations and optical gain

Using previous expressions obtained for the scattering rates in the presence/absence of magnetic field, we can write the expression for the total scattering rate of the system as

$$\frac{1}{\tau} = \frac{1}{\tau^{LO}} + \sum_{z_i} \left\langle \frac{1}{\tau^{IR}}(z_i) \right\rangle. \quad (18)$$

Finally, if one wants to compare the effects of electron-LO-phonon scattering and electron-interface roughness scattering, two things can be noted: (1) due to the nature of electron-interface roughness interactions, scattering rates for transition from lower to upper and from upper to lower energy level are equal. (2) the LO-phonon scattering has maximum influence when the energy difference between two states is close to phonon energy, $\Delta E_{LO} = \hbar\omega_{LO}$; on the other hand, the effects of interface roughness are maximal when the energy difference approaches zero. Therefore, the two mechanisms of scatterings are complementary.

When the magnetic field B is applied, continuous subbands E_n transform into discrete Landau levels. The expression for energies

$E_{n,l}$ is given by Ekenberg as [36]

$$E_{n,l} = E_n + (l + 1/2) \frac{\hbar e B}{m_{\parallel n}} + [(8l^2 + 8l + 5)\langle\alpha_0\rangle + (l^2 + l + 1)\langle\beta_0\rangle] \frac{e^2 B^2}{2\hbar^2}. \quad (19)$$

In Eq. (19), $m_{\parallel n}$ represents the parallel effective mass of the n th subband in the absence of the magnetic field [36], while α_0 and β_0 are the nonparabolicity parameters. The optical gain corresponds to transitions $(3, l) \rightarrow (2, l)$ and is given by [25,35]

$$g_{3 \rightarrow 2} = \frac{2e^2 \pi^2 d_{3 \rightarrow 2}^2}{\bar{n} \epsilon_0 \lambda} \sum_l \delta(E_{3,l} - E_{2,l} - \hbar\omega) (N_{3,l} - N_{2,l}), \quad (20)$$

where \bar{n} is the material refractive index, λ and ω denote the wavelength and the frequency of the emitted light, respectively, while $N_{3,l} - N_{2,l}$ represents the degree of population inversion. The Dirac function in the above equation is replaced in numerical calculations by a Lorentzian with the linewidth parameter $\Gamma = 4.25$ meV [37], $\delta(E_{3,l} - E_{2,l} - \hbar\omega) \rightarrow \frac{1}{\pi} \frac{\Gamma}{[E_{3,l} - E_{2,l} - \hbar\omega]^2 + \Gamma^2}$. The energy difference between states is dependent on the Landau index l , $E_{3,l} - E_{2,l} \approx E_3 - E_2 + (l + 1/2)\hbar e B \left(\frac{1}{m_{\parallel 3}} - \frac{1}{m_{\parallel 2}} \right)$. Therefore, the Dirac function (i.e. the Lorentzian) cannot be put in front of summation in Eq. (20). The transition matrix element is calculated as $d_{3 \rightarrow 2} = \int \eta_3^*(z) z \eta_2(z) dz$, where the wavefunctions η_n are found by solving the Schrödinger equation in the form [36]

$$\frac{d^2}{dz^2} \alpha_0 \frac{d^2 \eta_n}{dz^2} - \frac{\hbar^2}{2} \frac{d}{dz} \frac{1}{m} \frac{d \eta_n}{dz} + U(z) \eta_n = E_n \eta_n. \quad (21)$$

Here, m represents the effective mass at the conduction-band minimum.

To calculate the optical gain we need to find the inverse population which is the solution of a nonlinear system of rate equations:

$$N_i \sum_{j \neq i} \frac{\bar{f}_j}{\tau_{i \rightarrow j}} - \bar{f}_i \sum_{j \neq i} \frac{N_j}{\tau_{j \rightarrow i}} + \frac{J_i}{e} = 0, \quad (22)$$

where indices $i, j = 1, 2, \dots$ denote the electronic states sorted by energy and

$$\bar{f}_i = 1 - \frac{\pi \hbar}{e B} N_i \quad (23)$$

is the probability that the state i is not occupied according to the Fermi–Dirac distribution. The electrons arrive in the active region by a constant current, and they are injected only into a limited number of Landau levels of the excited laser state, i.e. levels $(3, 0), \dots, (3, l_{3,\max})$. The injection current can be represented as a sum of all currents J_i which inject electrons into levels $(3, l_3)$, and in a similar manner, the extraction current can be expressed as a sum of all currents J_i which extract the electrons from levels $(1, l_1)$. The energy values of maximal Landau levels for each subband described by $l_{1,\max}, l_{2,\max}$ and $l_{3,\max}$, are taken in this work to be roughly $E_{3,0} + 5k_B T$ and it is reasonable to assume that the levels above are almost empty, cf. [25].

In the absence of an external magnetic field, the electronic subbands have free particle-like energy dispersion in the direction parallel to the QW planes, which in the parabolic approximation reads as $E_{\parallel} = \hbar^2 k_{\parallel}^2 / 2m^*$, where m^* is the effective mass and k_{\parallel} is the in-plane wave vector. The non-radiative lifetime for the state $|3, k_{\parallel}\rangle$ is limited by the electron–LO-phonon scattering into the two lower subbands of the active region, and the optical gain may be described by the following expression:

$$g_{3,2} = \frac{e^2 \omega}{2\bar{n} \epsilon_0 c} \int_0^{+\infty} F_{3,2} |d_{3,2}|^2 \delta(E_3 - E_2 - \hbar\omega) d(k_{\parallel}^2), \quad (24)$$

where ϵ_0 is the vacuum dielectric permittivity, c is the speed of light in vacuum, $\hbar\omega$ is the photon energy, $F_{3,2}$ stands for the difference of Fermi–Dirac functions for the initial and the final state, while $d_{i,f} = \langle \eta_i | z | \eta_f \rangle$ is the transition matrix element, and η_i and η_f denote the z -dependent parts of the wave functions.

2.6. Optimization procedure of the QCL active region

In order to optimize the laser performance at selected wavelength, one must consider the entire free-parameters space and this type of search is best performed by some established method for global optimization, such as simulated annealing algorithm [38] employed in this work. This algorithm belongs to the class of stochastic global optimization methods and uses the Metropolis function for the acceptance probability. The annealing algorithm in each step randomly generates new configurations and calculates a fitness function value. Any downhill step is automatically accepted while an uphill step may be accepted according to the Metropolis criteria. The algorithm starts initially with annealing control parameter set to a high value, and as the annealing proceeds, the value of annealing control parameter declines. In this way, the system is expected to wander initially towards a broad region of the active parameter space containing good solutions and then the search towards minimum is narrowed down. One of the most important phases in the implementation of any simulated annealing algorithm is the selection of a formal fitness function, which should be defined to encompass the goals of optimization. Here, the objective is to optimize the optical gain at selected wavelength, hence the fitness function is taken in the following form [11]

$$F = - \frac{g(B=0)}{\left[\left(\frac{E_3 - E_2}{\hbar\omega} - 1 \right)^2 + \Theta^2 \right] \left[\left(\frac{E_2 - E_1}{\hbar\omega_{LO}} - 1 \right)^2 + \Theta^2 \right]}, \quad (25)$$

where the term in the denominator favors achieving specified emission wavelength (i.e. photon energy $\hbar\omega$) and the LO-phonon resonance. In addition, Θ is a nonzero constant, which ensures that F is strongly driven towards resonance in the course of optimization, while remaining finite at the exact resonance, and $g(B=0)$ is the optical gain in the absence of the magnetic field, given by Eq. (24). In numerical calculation, the optical gain can be expressed via the gain coefficient $g^* = (1 - \tau_{21}/\tau_{32})\tau_3 d_{32}^2$, where τ_{21} and τ_{32} are the scattering times and τ_3 is the upper laser level lifetime.

3. Program usage

In this section we provide instructions on how to operate the QCL program with a user-friendly graphical user interface (GUI) which was developed using MATLAB[®]. The QCL GUI enables the end user to easily manipulate the active region parameters, set and run simulations. The main m -file for running the program is *QCL.m*. The GUI has been designed so as to meet the following functions:

- The user can define her/his own input parameters, and to save them if desired. The user is able to choose only the input values within the allowed parameter range, see Table 1.
- The user is able to perform a search for the optimal QCL parameters for a given wavelength and temperature and to save the obtained values.
- The user is able to specify the range of magnetic field and visualize/save laser output properties in the presence of an external magnetic field.

Fig. 1 shows the graphical user interface. The window is basically divided into four panels. These panels are described in detail below.

Table 1
Summary of the input parameters and allowed range of values.

Parameter	Description	Minimum value	Maximum value
λ	Wavelength (μm)	5	15
T	Temperature (K)	1	350
Δ	IR scattering parameter (\AA)	0	2
Λ	IR scattering parameter (\AA)	0	200
X	Coefficient of $\text{Al}_x\text{Ga}_{1-x}\text{As}$ alloy composite	0.01	0.4
E	Electric field (kV/m)	3000	5000
<i>well</i> (1)	1st well width (\AA)	8^a	60
<i>barrier</i> (1)	1st barrier width (\AA)	8^a	60
<i>well</i> (2)	2nd well width (\AA)	8^a	60
<i>barrier</i> (2)	2nd barrier width (\AA)	8^a	60
<i>well</i> (3)	3rd well width (\AA)	8^a	60
<i>Bmin</i>	Lower endpoint of range of magnetic field (T)	3	60
<i>Bmax</i>	Upper endpoint of range of magnetic field (T)	3	60
<i>dB</i>	Step size for calculations in magnetic field (T)	/	/

^a If the system has two wells, one of the well or barrier widths is set to zero value, and other layer widths are in the range 8–60 \AA .

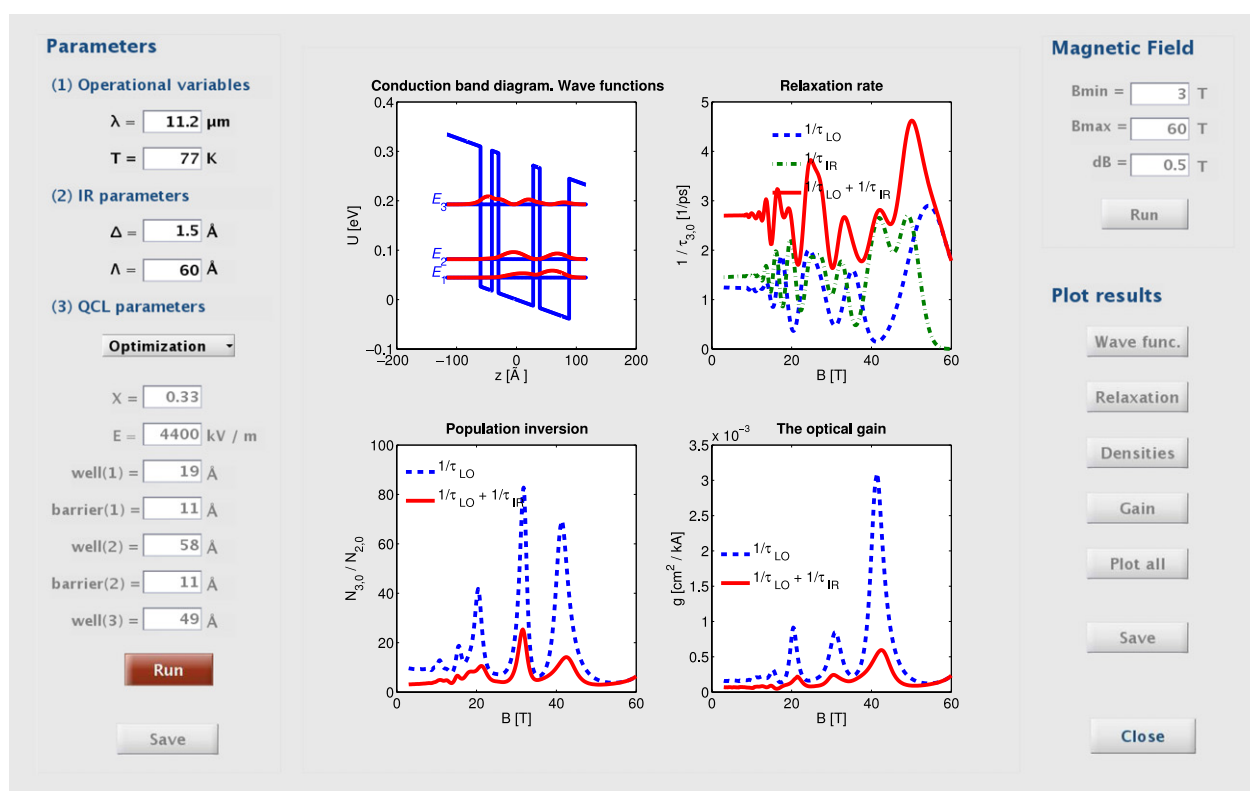


Fig. 1. QCL main window.

On the *Parameters* panel, there are three sub-panels. In the first two sub-panels, the input parameters are defined only by the user. In case of input entrance outside the allowed range (see Table 1), the parameter is automatically set to the closest allowed value or to NaN value (for example in case of text input). It is useful to note that if one of the IR parameters is chosen to be zero, the interface roughness scattering influence on the operation of QCL will not be considered. In the third *QCL parameters* sub-panel, the user has two options: (i) s/he can define the parameters manually, or (ii) s/he can optimize the laser performance at selected wavelength and temperature in the absence of magnetic field. If the optimization is selected, the ‘Run’ button will be enabled and after a click on this button alloy composition coefficient, electric field and layer widths lying in the appropriate range will be computed automatically using the simulated annealing algorithm. When the optimization is completed, calculated values will be entered in their boxes and the user will not be able to modify

these parameters. If s/he wants to modify or delete them, s/he has to select ‘Enter manually’ from the popup menu. The user can save the parameters. The ‘Save’ button is used for all input parameters of the *Parameters* panel. The input parameters are summarized in Table 1.

Once the QCL parameters are specified by using one of the above-mentioned ways, the user can calculate the scattering rates, the total relaxation rate, population inversion and the optical gain for a wide range of magnetic fields. On the *Magnetic field* panel, after defining the range of magnetic field, the user must click on the ‘Run’ button to analyze QCL dynamics when it is subjected to a magnetic field. After calculating QCL properties in magnetic field, the user can visualize results by clicking the appropriate button in the *Plot results* panel. Graphics appear in the central panel. The user can plot the active region of QCL, the total electron relaxation rate, the ratio of the total areal densities or the optical gain. There are options to plot a single graphic or to plot all the graphics together.

Table 2
Functions used for the optimization of QCL active region parameters.

Program	Description
QCLparam_opt.m	Finding optimal QCL parameters for given wavelength using annealing algorithm <i>calls:</i> fitness_fun.m, anneal.m
fitness_fun.m	Fitness function, function to be optimized (Eq. (25)) <i>inputs:</i> QCL parameters for optimization <i>calls:</i> QCLgain_opt.m
QCLgain_opt.m	Finding optical gain i.e. gain coefficient in the absence of the magnetic field (Eq. (24)) <i>inputs:</i> QCL parameters for optimization, wave functions, energy eigenvalues <i>calls:</i> WLO_opt.m, WIR_opt.m
WLO_opt.m	Finding LO-phonon scattering rate at zero magnetic field (Eq. (10)) <i>inputs:</i> wave functions, energy eigenvalues, temperature
WIR_opt.m	Finding IR scattering rate at zero magnetic field (Eq. (17)) <i>inputs:</i> energy eigenvalues, IR scattering parameters, width of the Gaussian distribution
anneal.m	Simulated annealing optimization method <i>inputs:</i> fitness function, initial values of parameters to be optimized

These graphics can be saved in the form of a picture file (.tif) by using the 'Save' button.

The 'Close' button on the right side of the GUI is a general button that closes the program and clears any temporary information.

4. Running the program and examples

In the following examples, applications of QCL program are presented. We illustrate how the program can be used to obtain (i) a gain-maximized structure and (ii) laser output properties in magnetic field.

4.1. Optimization of the QCL active region parameters

The first test run is concerned with the optimization of QCL active region parameters, described in the Section 2, by means of the simulated annealing algorithm. Here, we demonstrate the optimization of QCL active region parameters at two wavelengths $\lambda = 10 \mu\text{m}$ and $\lambda = 11 \mu\text{m}$.

An overview of the principal functions used for optimization is given in Table 2. The principal script is *QCLparam_opt.m*. The parameters m_{GaAs} and m_{AlAs} are defined in *param1.m*. The dielectric permittivities used in numerical calculations ϵ_{∞} , ϵ_s and the width δ are defined in *phyconst.m*. Nonparabolicity parameters α_1 and β_1 are defined in *param2.m*.

Starting from the predefined initial values of active region parameters, we minimize the fitness function given by Eq. (25) using the simulated annealing algorithm [38]. The optimization time on Intel 3 GHz processor is about 2×10^4 s. The QCL configurations with corresponding wave functions squared, obtained using the optimization algorithm, are given in Fig. 2(a) and (b). The structural parameters for the QCL active region for $\lambda = 10 \mu\text{m}$ are 25, 30, 59, 12 and 59 Å (for the well and the barrier widths, respectively, going from left to right) and the applied electric field in the z direction is $E = 3581$ kV/m. The obtained Al mole fraction is $X = 0.4$, so the structure may be realized by GaAs/Al_{0.4}Ga_{0.6}As. Another optimization is performed for $\lambda = 11 \mu\text{m}$, and the optimization procedure has delivered a structure with the following layer widths: 26, 23, 58, 12, 51 Å. The applied electric field is $E = 4600$ kV/m and Al mole fraction $X = 0.37$.

Table 3
Functions used for calculation of the output characteristics of QCL in the magnetic field.

Program	Description
main1.m	Finding subband positions at zero magnetic field and corresponding wave functions <i>calls:</i> phyconst.m, param1.m, shooting.m
main2.m	Finding scattering rates, the total relaxation rates, population inversion and the optical gain in the presence of an intense external magnetic field <i>calls:</i> phyconst.m, param1.m, param2.m, dipol.m, GQP.m, Ekenberg.m, WLO.m, WIR.m, iterrateequ.m, gainQCL.m
shooting.m	Shooting method for the Schrödinger equation <i>inputs:</i> energy eigenvalue
dipol.m	Calculation of dipole (transition matrix) element <i>inputs:</i> wave functions, energy eigenvalues, parallel masses
GQP.m	Calculation of form factor <i>inputs:</i> wave functions, in-plane component of the phonon wave vector
Ekenberg.m	Energies given by Ekenberg (Eq. (19)) <i>inputs:</i> energy eigenvalue, parallel mass, magnetic field
WLO.m	Finding LO-phonon scattering rate (Eq. (5)) <i>inputs:</i> energy eigenvalues, form factor, in-plane component of the phonon wave vector, magnetic field, temperature, width of the Gaussian distribution
WIR.m	Finding IR scattering rate (Eq. (14)) <i>inputs:</i> energy eigenvalues, magnetic field, IR scattering parameters, width of the Gaussian distribution
iterrateequ.m	Calculation of inverse population which is obtained from the solution of a nonlinear system of rate equations (Eq. (22)) <i>inputs:</i> scattering rate, distribution of current, magnetic field
gainQCL.m	Calculation of the optical gain (Eq. (20)) <i>inputs:</i> energy eigenvalues, inverse population, dipole element

4.2. Output characteristics of QCL in magnetic field

This section presents calculations of the output characteristics of QCL in the presence of an external magnetic field. The aim of this example is to demonstrate how the optical gain, resulting from the combined action of LO-phonon and IR scattering mechanisms, is influenced by varying the magnetic field strength. The overview of the scripts and functions is given in Table 3.

Each run has a set of unique parameters associated with it, including wavelength, temperature, IR scattering parameters, the alloy composition coefficient, electric field and layer widths. In the first calculation, we use parameters previously obtained by optimization at $\lambda = 10 \mu\text{m}$. In Fig. 3(a) and (b) the relaxation rates for the low temperatures ($T = 77$ K) and the room temperature ($T = 300$ K) are shown, respectively. The first bottleneck of simulation is calculation of the form factor, cf. Eq. (7). This takes roughly 3×10^3 s at 3 GHz processor. After that, relaxation rates are calculated for every energy level within subbands. Since the number of levels is inversely proportional to the applied magnetic field and three subbands are involved, the calculation time decreases as B^{-2} with magnetic field. Calculation time at $B = 10$ T on Intel 3 GHz processor is about 600 s. Oscillations of the relaxation rate with B are very pronounced, and very prominent peaks are found at values of the magnetic field which satisfy the resonance conditions for LO-phonon emission. If the relaxation rates due to interface roughness and LO-phonon scattering are compared, one can see that the local relaxation rate maxima are of the same order of magnitude and not correlated with respect to the applied magnetic field. This is due to the fact that interface roughness scattering has the largest influence when the energy difference between states is diminishing. In contrast, for LO-phonon scattering, when the arrangement

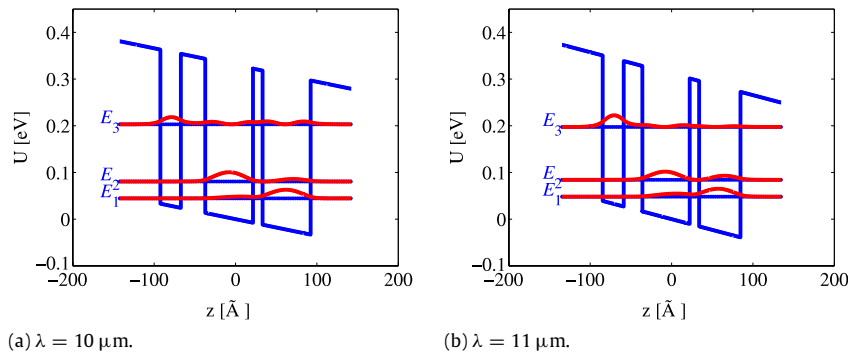


Fig. 2. (a) The active region of QCL, optimized for emission at $\lambda = 10 \mu\text{m}$. (b) The active region of QCL, optimized for emission at $\lambda = 11 \mu\text{m}$.

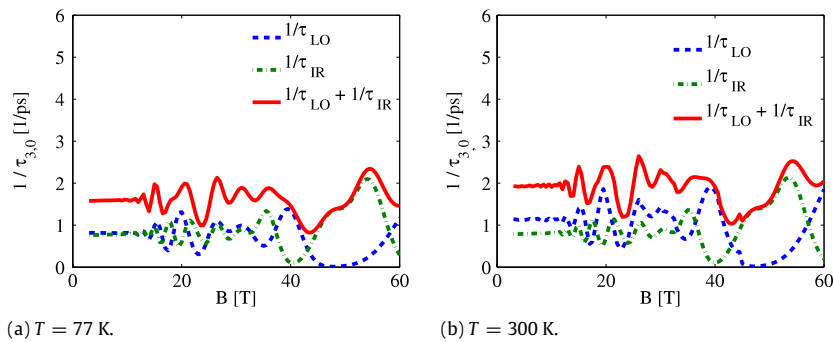


Fig. 3. The total electron relaxation rate due to the electron LO-phonon scattering and interface roughness scattering for transitions from the ground laser level of the third subband into the two sets of Landau levels of the lower subbands, for the magnetic fields in the range of $B = 3\text{--}60 \text{ T}$ and at temperature (a) $T = 77 \text{ K}$ and (b) $T = 300 \text{ K}$. The QCL active region parameters used are obtained by optimization at $\lambda = 10 \mu\text{m}$. The IR scattering parameters used in calculation are $\Delta = 60 \text{ \AA}$ and $\Lambda = 1.5 \text{ \AA}$.

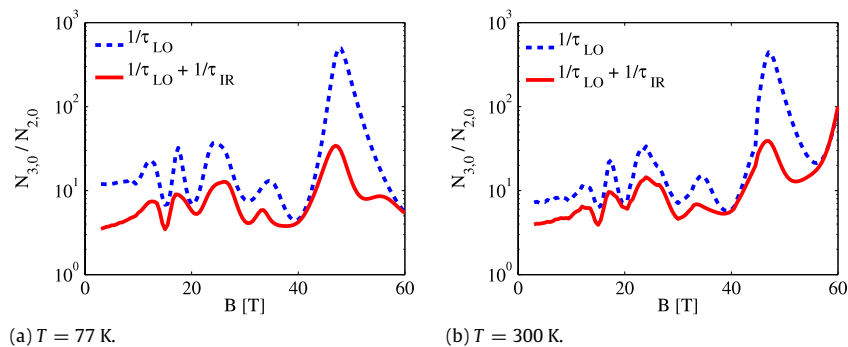


Fig. 4. The ratio of the total electron areal densities due to the electron LO-phonon and interface roughness scattering, in the ground laser levels of the third and the second subband, for the magnetic fields in the range of $B = 3\text{--}60 \text{ T}$ and at temperature (a) $T = 77 \text{ K}$ and (b) $T = 300 \text{ K}$. The QCL active region parameters used are obtained by optimization at $\lambda = 10 \mu\text{m}$. The IR scattering parameters used in calculation are $\Delta = 60 \text{ \AA}$ and $\Lambda = 1.5 \text{ \AA}$.

of laser levels is such that there is a level situated at $\hbar\omega_{LO}$ below the state $(3, 0)$, this type of scattering is enhanced. One can also see that the peaks at magnetic fields $B < 20 \text{ T}$ are a result of combined action of two scattering mechanisms. Assuming a constant current injection, the modulation of lifetimes of all the states in the system results in either suppression or an enhancement of population inversion between states $(3, 0)$ and $(2, 0)$, see Fig. 4(a) and (b).

In Fig. 5, the optical gain is shown at three wavelengths $\lambda = 9, 10, \text{ and } 11 \mu\text{m}$. The QCL active region parameters are obtained by optimization at $\lambda = 10 \mu\text{m}$. One can observe significant changes in the magnitude of the optical gain, but at the same time, the gain as a function of magnetic field looks qualitatively similar for different (close by) wavelengths. The difference in magnitude of the gain is about one order of magnitude between resonant wavelength $\lambda = 10 \mu\text{m}$ and other two wavelengths $\lambda = 9, 11 \mu\text{m}$. Finally, we should note that the QCL operating in the mid-IR spectral range was chosen to demonstrate our simulation code since experimental data were readily available [6].

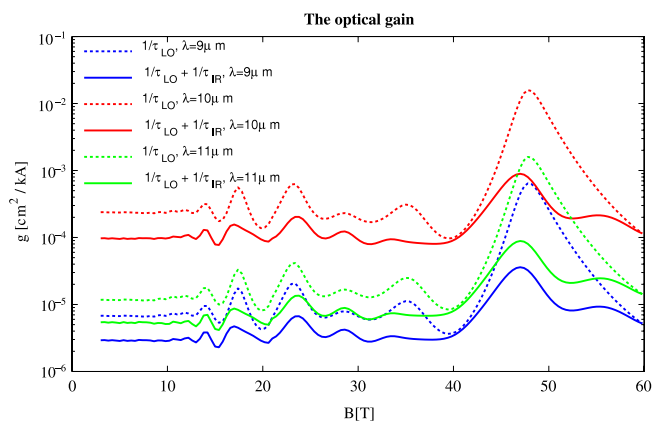


Fig. 5. The optical gain (per unit injection current) as a function of the applied magnetic field in the range $B = 3\text{--}60 \text{ T}$, at temperature $T = 77 \text{ K}$.

5. Conclusion

MATLAB[®]-based program is introduced, which solves the rate equations-based model and analyzes the optical gain in the active region of a QCL in magnetic field perpendicular to the layers of the structure. The scattering on both LO-phonons and interface roughness is included in modeling. Magnetic field alters the number of relevant in-plane electronic levels and the corresponding relaxation rates between them, by positioning some states on or off resonance with the upper laser level. Scattering effects are also important for relaxation of electrons from the second level to the first (ground) level. While interface roughness relaxation has maximal effects when the energy difference between levels is negligible, the LO-phonon scattering is enhanced if energy difference is close to resonant phonon energy. It is evident from the obtained numerical results that the inclusion of interface roughness scattering does not introduce additional (strong) peaks of inverse population and optical gain with varying magnetic field, it mainly affects their magnitude. The work aims to distribute an open source program which can be easily understood, used for efficient modeling and understanding of QCL operation and/or straightforwardly modified for the THz spectral range.

Acknowledgments

The authors acknowledge support by the Ministry of Education and Science of the Republic of Serbia under Projects No. ON171017, III45018, III45010 and NATO SfP Grant, ref. no. ISEG.EAP.SFPP 984068. Numerical simulations were developed and tested on the AEGIS e-Infrastructure, supported in part by FP7 projects EGI-InSPIRE, PRACE-1IP, PRACE-2IP, and HPSEE.

References

- [1] A.Y. Cho (Ed.), *Molecular Beam Epitaxy*, American Institute of Physics AIP Press, New York, 1994.
- [2] L. Esaki, R. Tsu, *IBM J. Res. Dev.* 14 (1970) 61.
- [3] J. Faist, F. Capasso, D.L. Sivco, C. Sirtori, A.L. Hutchinson, A.Y. Cho, *Science* 264 (1994) 553.
- [4] C. Gmachl, F. Capasso, D.L. Sivco, A.Y. Cho, *Rep. Progr. Phys.* 64 (2001) 1533.
- [5] C. Becker, C. Sirtori, O. Drachenko, V. Rylkov, D. Smirnov, J. Leotin, *Appl. Phys. Lett.* 81 (2002) 2941.
- [6] D. Smirnov, O. Drachenko, J. Leotin, H. Page, C. Becker, C. Sirtori, V. Apalkov, T. Chakraborty, *Phys. Rev. B* 66 (2002) 125317.
- [7] D. Smirnov, C. Becker, O. Drachenko, V.V. Rylkov, H. Page, J. Leotin, C. Sirtori, *Phys. Rev. B* 66 (2002) 121305.
- [8] A. Leuliet, A. Vasanelli, A. Wade, G. Fedorov, D. Smirnov, G. Bastard, C. Sirtori, *Phys. Rev. B* 73 (2006) 085311.
- [9] A. Bismuto, R. Terazzi, B. Hinkov, M. Beck, J. Faist, *Appl. Phys. Lett.* 101 (2012) 021103.
- [10] M.T. Arafin, N. Islam, S. Roy, S. Islam, *Opt. Quantum Electron.* 44 (2012) 701.
- [11] A. Daničić, J. Radovanović, V. Milanović, D. Indjin, Z. Ikonić, *J. Phys. D: Appl. Phys.* 43 (2010) 045101.
- [12] A. Mirčetić, D. Indjin, Z. Ikonić, P. Harrison, V. Milanović, R.W. Kelsall, *J. Appl. Phys.* 97 (2005) 084506.
- [13] D. Indjin, S. Tomić, Z. Ikonić, P. Harrison, R.W. Kelsall, V. Milanović, S. Kočinac, *Appl. Phys. Lett.* 81 (2002) 2163.
- [14] S. Tomić, M. Tadić, V. Milanović, Z. Ikonić, *J. Appl. Phys.* 87 (2000) 7965.
- [15] B.S. Williams, *Nat. Photonics* 1 (2007) 517.
- [16] O. Drachenko, S. Winnerl, H. Schneider, M. Helm, J. Wosnitza, J. Leotin, *Rev. Sci. Instrum.* 82 (2011) 033108.
- [17] A. Hugi, R. Maulini, J. Faist, *Semicond. Sci. Technol.* 25 (2010) 083001.
- [18] R.F. Curl, F. Capasso, C. Gmachl, A.A. Kosterev, B. McManus, R. Lewicki, M. Pusharsky, G. Wysocki, F.K. Tittel, *Chem. Phys. Lett.* 487 (2010) 1.
- [19] M. Tonouchi, *Nat. Photonics* 1 (2007) 97.
- [20] C. Becker, A. Vasanelli, C. Sirtori, G. Bastard, *Phys. Rev. B* 69 (2004) 115328.
- [21] A. Wade, G. Fedorov, D. Smirnov, S. Kumar, B.S. Williams, Q. Hu, J.L. Reno, *Nat. Photonics* 3 (2009) 41.
- [22] G. Scalari, C. Walther, L. Sirigu, M.L. Sadowski, H. Beere, D. Ritchie, *Phys. Rev. B* 76 (2007) 115305.
- [23] F.R. Jasnot, et al., *Appl. Phys. Lett.* 100 (2012) 102103.
- [24] G. Scalari, et al., *Appl. Phys. Lett.* 97 (2010) 081110.
- [25] J. Radovanović, V. Milanović, Z. Ikonić, D. Indjin, P. Harrison, *J. Appl. Phys.* 97 (2005) 103109.
- [26] M. Žeželj, V. Milanović, J. Radovanović, I. Stanković, *J. Phys. D: Appl. Phys.* 44 (2011) 325105.
- [27] H.B. Teng, J.P. Sun, G.I. Haddad, M.A. Stroschio, S. Yu, K.W. Kim, *J. Appl. Phys.* 84 (2008) 2155.
- [28] A.P. Prudnikov, Yu.A. Brychkov, O.I. Marichev, *Integrals and Series: More Special Functions*, Vol. 3, Gordon and Breach, New York, 1990.
- [29] A. Valavanis, Z. Ikonić, R.W. Kelsall, *Phys. Rev. B* 77 (2008) 075312.
- [30] T. Unuma, T. Takahashi, N. Takeshi, M. Yoshita, T. Noda, H. Sakaki, M. Baba, H. Akiyama, *Appl. Phys. Lett.* 78 (2001) 3448.
- [31] C. Weisbuch, R. Dingle, A.C. Gossard, W. Wiegmann, *Solid State Commun.* 38 (1981) 709.
- [32] T. Ando, A.B. Fowler, F. Stern, *Rev. Modern Phys.* 54 (1982) 437.
- [33] T. Unuma, M. Yoshita, T. Noda, H. Sakaki, H. Akiyama, *J. Appl. Phys.* 93 (2003) 1586.
- [34] N. Califano, et al., *Phys. Rev. B* 75 (2007) 045338.
- [35] S. Živanović, V. Milanović, Z. Ikonić, *Phys. Rev. B* 52 (1995) 8305.
- [36] U. Ekenberg, *Phys. Rev. B* 40 (1989) 7714.
- [37] J. Wang, J.-P. Leburton, Z. Moussa, F.H. Julien, A. Sa'ar, *J. Appl. Phys.* 80 (1996) 1970.
- [38] S. Kirkpatrick, C.D. Gelatt, M.P. Vecchi, *Science* 220 (1983) 4598.